PCCP

Accepted Manuscript

ROYAL SOCIETY OF CHEMISTRY

www.rsc.org/pccp

Physical Chemistry Chemical Physics
CREATED USING THE RSC LaTeX PCCP ARTICLE TEMPLATE – SEE www.rsc.org/electronicfiles FOR DETAILS
ARTICLE TYPE www. rsc.org/xxxxxx | XXXXXXXX

Unexpected strong magnetism of Cu doped single-layer MoS_2 and its origin

Won Seok Yun[ab] **and J. D. Lee**[*a]

Received Xth XXXXXXXXXX 20XX, Accepted Xth XXXXXXXXX 20XX
First published on the web Xth XXXXXXXXXX 200X
DOI: 10.1039/b000000x

Magnetism of the 3*d* transition-metal (TM) doped single-layer (1L) MoS_2, where Mo atom is partially replaced by the 3*d* TM atom, is investigated using the first-principles density functional calculations. In a series of 3*d* TM doped 1L-MoS_2's, the induced spin polarizations are negligible for Sc, Ti, and Cr dopings, while the induced spin polarizations are confirmed for V, Mn, Fe, Co, Ni, Cu, and Zn dopings and the systems become magnetic. Especially, the Cu doped system shows unexpectedly strong magnetism although Cu is nonmagnetic in its bulk state. The driving force is found to be a strong hybridization between Cu 3*d* states and 3*p* states of neighboring S, which results in an extreme unbalanced spin-population in the spin-split impurity bands near the Fermi level. Finally, we also discuss further issues of the Cu induced magnetism of 1L-MoS_2 such as investigations of additional charge states, the Cu doping at S site instead of Mo site, and the Cu adatom on the layer (i.e., 1L-MoS_2).

1 Introduction

Enormous research efforts have been focused on the layered transition-metal (TM) dichalcogenides due to their potential applicability as a promising nanoscopic building block in areas such as lubrication, catalysis, electrochemical photocells, lithium ion battery, and so on.[1–5] Especially, among those, molybdenum disulfide (MoS_2) can amplify electrical signals at room temperature by consuming much less power than traditional silicon. Structurally, MoS_2 exhibits a sandwich type of covalently bonded S-Mo-S two-dimensional hexagonal planes, which are bound together by weak van der Waals forces in the bulk.[6] Intriguingly, the electronic structure of MoS_2 shows a strong dependence on the layer thickness and strain.[7–9] A single-layer (1L) MoS_2, which is obtained by employing the microexfoliation,[10] is particularly interesting. 1L-MoS_2 is a direct gap semiconductor with a band gap (E_g) of $\sim$1.8 eV, whereas the bulk MoS_2 is an indirect gap semiconductor with E_g $\sim$1.3 eV.[7,8,11] A sizable band gap of 1L-MoS_2 enables wide electronic applications such as transistors, photodetectors, and electroluminescent devices.[12–14]

Recently, considerable attention has been paid to the magnetic properties of this material for the spintronic applications.[15,16] Numerous theoretical studies have shown that not only the bulk MoS_2 but also a few-layer (*n*L-) or 1L-MoS_2 exhibit diamagnetism. However, MoS_2 becomes ferromagnetic (FM) in the cases of nanoribbon with zigzag edges, passivation with hydrogen, vacancy defect formation, adsorption or substitutional doping of nonmetal or TM elements, and even quasi-one-dimensional nanowires.[17–24] Several experimental studies have been done in a relation to the magnetism of MoS_2.[25–29] Komsa et al.[26] demonstrated the vacancy formation in MoS_2 under exposure to 80 keV electron-beam irradiation and then the vacancy filling with substitutional impurity atoms. This doping scheme provides a new opportunity to modify the fundamental properties of MoS_2. Note that the scheme has also been applied to other materials like carbon nanotube, graphene, and boron nitride.[30,31] In addition, it has been also demonstrated experimentally that the pulsed laser deposition can be used to dope graphene by single TM atoms such as Pt, Co, and In.[32] The Curie temperature (T_C) reaches up to 895 K in MoS_2 which was irradiated by 2 MeV proton-beam[27] and also the weak ferromagnetism (1-2 emu/g) with T_C of 685 K was observed in the edge-oriented MoS_2 nanosheet film.[28] Moreover, it was observed that the hydrogenation of MoS_2 leads to the magnetic easy axis of out-of-plane, while the proton irradiation leads to the easy axis of in-plane.[29] This provides a new experimental method for the manipulation of magnetic easy axis of MoS_2. Very recently, there were theoretical reports that the 1L-MoS_2 doped by some of TM atoms (such as V, Mn, Fe, Co, Ni, Zn, Cd, and Hg) were magnetic.[33–36] However, a clear understanding for the induced magnetism in those systems has not been made yet.

In order to fully understand and control the magnetic properties of the MoS_2 thin films with the impurity atom as dopant, a systematic theoretical study is required. In the present paper, we examine the electronic and magnetic properties of a series of 3*d* TM doped 1L-MoS_2's - one 3*d* TM atom is substituted

[a] *Department of Emerging Materials Science, DGIST, Daegu 711-873, Korea. E-mail: jdlee@dgist.ac.kr*
[b] *Center for X-ray Optics, Lawrence Berkeley National Laboratory, Berkeley, CA 94720, USA*

for one of Mo atoms in the supercell - in a systematic fashion with the first-principles electronic structure calculation. Notably, we find that the Cu doped 1L-MoS_2 have an unexpectedly large spin magnetic moment of up to 5.08 μ_B per supercell even if Cu is nonmagnetic (NM) in its bulk state. This casts an interesting but puzzling problem how the magnetism develops in the environment of 1L-MoS_2 accompanying NM TM elements. We explore the driving force for the induced magnetism, which is attributed to the strong hybridization between Cu 3*d* states and 3*p* states of neighboring S and the resulting spin-split impurity bands. This understanding should provide seminal information about the origin of magnetism in the 3*d* TM doped 1L-MoS_2. Finally, to gain deeper insight into the Cu induced magnetism, we also discuss some of further issues such as investigations of additional charge states, Cu doping at S sites instead of Mo sites, and Cu adatom on the layer.

2 Computational Details

In the present calculation, in order to investigate the different concentration of 3*d* TM atoms, we consider models of the 3×3, $2\sqrt{3} \times 2\sqrt{3}$, 4×4, and 5×5 supercells for 1L-MoS_2, where one of Mo atoms of the supercell is replaced by one 3*d* TM atom. The models correspond to 11.11, 8.33, 6.25, and 4.00 at.% of 3*d* TM in 1L-MoS_2, respectively. First-principles electronic structure calculations are performed using the Vienna *ab-initio* simulation package (VASP)[37] with projector-augmented wave (PAW) pseudopotentials,[38] where spin-polarized generalized gradient approximation (GGA) of Perdew-Bruke-Ernzerhof (PBE) functional[39] was employed for the exchange-correlation potential. Experimentally measured lattice constants of the bulk MoS_2 (a = 3.16 Å) in the lateral direction are adopted and all atomic positions are fully optimized using the conjugate gradient method, where the total energy and atomic forces are minimized. A vacuum region more than 15 Å is used to ensure decoupling between neighboring slabs. A plane-wave basis set with the cutoff energy of 450 eV is used for all the considered systems. An integration over the Brillouin zone is carried out by using $8 \times 8 \times 1$ Monkhorst-Pack **k**-point mesh for the 2×2 and $2\sqrt{3} \times 2\sqrt{3}$ supercells, $6 \times 6 \times 1$ mesh for the 4×4 supercell, and $4 \times 4 \times 1$ mesh for the 5×5 supercell, respectively. The local magnetic moments, the spin-density, and the partial density of states (PDOS) were calculated within the Wigner-Seitz (WS) radius of each atom, which is chosen based on PBE potentials implemented in the VASP code.

3 Results and Discussion

3.1 Formation stability

We firstly calculate the formation enthalpy ΔH of the 3*d* TM doped 1L-MoS_2 for the understanding of its relative stability. Note that the obtained total energy is the internal energy U at zero Kelvin and zero pressure. At this condition, the formation enthalpy is simply the internal energy. It reads as follows:

$$\Delta H = \frac{H(\mathrm{Mo}_l\mathrm{TM}_m\mathrm{S}_n) - lH(\mathrm{Mo}) - mH(\mathrm{TM}) - nH(\mathrm{S})}{l+m+n}, \quad (1)$$

where $H(\mathrm{Mo}_l\mathrm{TM}_m\mathrm{S}_n)$ is the enthalpy of $\mathrm{Mo}_l\mathrm{TM}_m\mathrm{S}_n$ system and l, m, and n are the numbers of Mo, 3*d* TM, and S atoms, respectively. H(Mo), H(TM), and H(S) are the enthalpy per atom of the body centered cubic Mo, 3*d* TM in its ground state structure, and orthorhombic α-S, respectively.

In Fig. 1, we present the results of calculated ΔH values using Eq. (1) for the 3*d* TM doped 1L-MoS_2. As displayed in the figure, ΔH of all the doped systems are found to be higher than that of the pristine 1L-MoS_2 which is estimated to be -0.974 eV/atom (as a dotted horizontal line). For the bulk MoS_2, ΔH is calculated to be -0.959 eV/atom, which is similar to that of the pristine 1L-MoS_2. This is also in good agreement with the experimentally observed ΔH (-272 kJ/mol = -0.940 eV/atom).[40] The formation enthalpy gradually decreases with decreasing the 3*d* TM concentration (generally, smaller value of ΔH (< 0) implies more stable formation). Being directly related to the present work, an experimental Co doping can be achieved at the MoS_2 edge by sulfidation of the mixture of ammonium heptamolybdate and cobalt nitrate.[41] Therefore, it is expected that the same chemical approach could be applied to the Cu doping in place of Mo in MoS_2, which has the maximum value of ΔH among 3*d* TM impurities. One can find that the difference of ΔH between Co- and Cu-dopant cases is relatively small (43 meV/atom). Therefore, all the relevant values of ΔH are in fact negative, which signifies that a stable formation of the corresponding systems will be still possible.

3.2 Magnetism

The local magnetic moments of 3*d* TM, Mo, and S atoms and the interstitial magnetic moment (being associated with charges outside WS radius) in the considered systems are plotted with respect to a series of 3*d* TM atoms for four different TM concentrations in Fig. 2. Mo and S atoms in the figure represent those surrounding one 3*d* TM atom in the 3*d* TM doped MoS_2. In the cases of Sc, Ti, and Cr doped systems, the induced spin polarization are almost negligible for all the doping concentration, whereas the rest are found to be actually magnetic. Moreover, one can see from the Fig. 2. that most of the magnetism comes from the 3*d* TM atom and the

interstitial part of the system. The magnetic TM dopants like Fe, Co, and Ni which are FM in their bulk states show 1.18 μ_B/Fe, 0.94 μ_B/Co, and 1.23 μ_B/Ni at 6.25 at.%, respectively. They also induce moderate sizes of magnetic moments at Mo and S surrounding them and in the interstitial area. In contrast, interestingly, although Cu is NM in its bulk state, the Cu doping leads to an appreciable magnitude of the moment, i.e., 0.55 μ_B/Cu at 6.25 at.% together with noticeable magnitudes of induced moments of 0.30 and 0.23 μ_B/atom at Mo and S, respectively. It is further interesting that a Cu doping results in the largest interstitial magnetic moment among 3*d* TM doped 1L-MoS_2's. The interstitial magnetic moment in the Cu doped case amounts to 1.06 μ_B/supercell, which can be compared to 0.12, −0.02, 0.09, 0.29, 0.70, and 0.38 μ_B/supercell for V, Mn, Fe, Co, Ni, and Zn doped cases at 6.25 at.%, respectively. Meanwhile, it is noticed that the magnetic moments displayed in Fig. 2 hardly change for the TM concentrations lower than 8.33 at.%. This means that the supercell size larger than $2\sqrt{3} \times 2\sqrt{3}$ has actually no more significant effect on the magnetic properties of the 3*d* TM doped 1L-MoS_2. Therefore, we hereafter focus on the 4×4 supercell except for Sc, Ti, and Cr cases, corresponding to the TM concentration of 6.25 at.%, unless mentioned otherwise.

To visualize the detailed distribution of magnetic moments of the 3*d* TM doped 1L-MoS_2, we plot the spin-density isosurfaces in Fig. 3. For V, Mn, and Fe doped systems, the spin-density is found to be localized mainly at the 3*d* TM atom. Particularly, in the Mn doped 1L-MoS_2, the neighboring S atoms are antiferromagnetically coupled to the Mn atom [see Fig. 3 (b)]. On the other hand, in the cases of Co, Ni, Cu, and Zn doped systems, appreciable spin-densities are distributed on the six nearest neighbors (S atoms) and the six second-nearest neighbors (Mo atoms) to the 3*d* TM atom, as shown in Fig. 3. Furthermore, in these cases, a sizable portion of the spin-density resides in the interstitial remnant space between the nearest neighbors and the second-nearest neighbors surrounding the TM atom. Spin-density isosurfaces in the figure readily confirm that the Cu doping results in the largest interstitial magnetic moment among 3*d* TM doped 1L-MoS_2's. The interstitial magnetic moments could give an insight that the hybridization between TM and neighboring S atoms would play a role in the induced magnetism, which may tell us that the hybridization might be stronger in Co, Ni, Cu, and Zn doped systems than in V, Mn, and Fe doped systems. This will be explicitly discussed in the next section.

3.3 Origin of magnetism

There have been reports that the lattice distortion or strain due to defects may induce the magnetism. For instance, the lattice strain due to O vacancy induces the ferromagnetism in TiO_2 [42] and Zn vacancy defect induces the ferromagnetism in ZnO.[43] Similarly, in the present case, the atomic relaxation will occur in the substitutional doping of a 3*d* TM for a single Mo atom. In Table I, the total magnetic moments are compared between the relaxation-allowing (relaxed) and relaxation-quenching (unrelaxed) calculations. For the unrelaxed calculation, we fix the bond length ($l_{\text{TM-S}}$ = 2.41 Å) and the bond angle ($\theta = 40.76^\circ$) as those for the pristine 1L-MoS_2. The bond length and angle turn out to be actually sensitive to the atomic relaxation. Nevertheless, the total magnetic moments are not substantially affected by the atomic relaxation according to Table I. However, the only exception is for V. Hence, the atomic relaxation should be ruled out as the origin of the largest interstitial magnetic moment and eventually the largest total magnetic moment of the Cu doped 1L-MoS_2.

In order to explore the origin of magnetism in another respect, we examine the electronic DOS. In Fig. 4, we illustrate the total and interstitial DOS. The interstitial DOS, which is associated with the charges outside WS radii, is estimated by the difference between the total DOS and a sum of all PDOS (within WS radii). As seen in the figure, except for the V doped case which is quite similar to the pristine case, the band hybridization results near the Fermi level and the impurity bands due to 3*d* TM dopings are created, which obviously contribute to DOS in the interstitial region. These impurity bands induce the spin-splitting and gradually shift from the conduction band minimum (CBM) to the valance band maximum (VBM) as the atomic number increases from Mn to Cu. This leads to a linear increase of the total magnetic moments from Mn to Cu, i.e., with respect to the *d* orbital occupancy, as in Table I. In the case of Zn, however, this trend is not followed. Very recently, to understand the induced magnetic moments in the TM doped MoS_2, the simple electron-counting approach has been considered using the first-principles calculation.[34,36] For example, in the case of the Mn doped 1L-MoS_2, the Mn substitution leads to localized states (impurity bands) within the band gap. The Mn 3*d* orbitals split into a single a_1 (d_{z^2}) state and two twofold degenerate e_1 (d_{xz/x^2-y^2}) and e_2 ($d_{xz/yz}$) since the Mn atom under the crystal field has the C_{3v} symmetry. In a simple ionic scenario, an additional valence electron in Mn (compared to Mo) should result in only the $a_1^{\uparrow}$ state being occupied, which has a magnetic moment of 1 μ_B/Mn atom.[34,36] Our present results are also in good agreements with that, as shown in Fig. 4.

Now, we can apply the approach to the V or Cu doped MoS_2 of our present study. Elucidation is enabled by investigating the PDOS of the *d*- and *p*-states of the V and Cu doped systems, which have comparatively weak and strong magnetism, in Figs. 5 (a) and (b). An isolated V atom has a $3d^3 4s^2$ configuration with one electron less than Mo atom. The impurity bands are too close to the VBM [see Fig. 5 (a)]. Only a_1 (d_{z^2}) state in the majority spin is occupied, while that in minority spin is pushed away above the Fermi level. In addition, no

significant hybridization between them near the Fermi level could be found so that only the a_1 state of V atom has weak spin-splitting in the vicinity of the Fermi level. As a result, the calculated magnetic moment leads to $\sim$1 μ_B/supercell. On the other hand, the impurity bands of the Cu 3*d* state split into three states as shown in Fig. 5(b). Interestingly, all (a_1, e_1, and e_2) of the impurity bands in the majority spin state are completely occupied, while all of those in the minority spin state are pushed above the Fermi level. These states of Cu atom hybridize strongly with *p* states of neighboring S atoms. Among those TM doped systems, note that the spin-splitting of the Cu doped system near the Fermi level is most dramatic. This should result in the magnetic moment of $\sim$5 μ_B/supercell.[44]

Next, we may need to think of the fundamental mechanism of the observed strong magnetism. Unusual magnetism in various diluted magnetic semiconductor compounds used to be explained by the similar *p-d* hybridization.[45] The original form of this *p-d* exchange interaction would be also related to that by Kanamori and Terakura,[46] which may serve as a probable candidate in the present Cu doped 1L-MoS_2. In contrast, the double-exchange interaction may be also considered as another candidate.[35] In the sense, the fundamental mechanism for the ferromagnetic ordering still remains veiled. Further study including the many body investigation will be required to answer this question.

3.4 Further issues of Cu induced magnetism

In Fig.6, we display the total magnetic moment and the energy difference between FM and NM states with respect to the number of net charges per supercell. First, it is found that FM states are energetically favored over NM states in the whole range of additional charges from $-3e$ to $3e$. Second, the total magnetic moments are found to decrease linearly as the net charges (whether negative or positive) are added to the neutral state. In a limited sense, it can be understood from the rigid band model based on the total DOS of the neutral state like in Fig.4 (especially, the total DOS near the Fermi level). For the negative charge increment, the Fermi level is pushed upward and the minority DOS increases, which leads to a decrease of the magnetic moment (i.e., the magnetic moment corresponds to the difference between the majority and minority DOS). Similarly, for the positive charge increment, the Fermi level is pulled downward and the majority DOS decreases. This also gives a decrease of the magnetic moment. Thus, an understanding about the change of the magnetism depending on the charged state is possible in terms of the simple electron-counting from the DOS analysis and the rigid band picture.

The site-dependence of Cu doping (i.e., substitutional doping) is investigated by examining the Cu doping at S sites instead of Mo sites. Similarly to the previous sections, the calculation is performed for the 4×4 supercell of 1L-MoS_2 with one Cu atom substitution in the S site as illustrated in Fig. 7(a). Differently from Fig. 3(f) (i.e., with one Cu atom substitution in the Mo site), the spin-density is found to be localized mostly at the doped Cu atom and its three nearest neighbors (Mo atoms). The calculated local magnetic moments are 0.08 and 0.24 μ_B/atom for the Cu and Mo, respectively, so that the total magnetic moment amounts to 1.03 μ_B/supercell. Therefore, the magnetism is relatively weak compared to the Cu doping at Mo sites in 1L-MoS_2 (5.08 μ_B/supercell).

Finally, the systems of Cu adatom on 1L-MoS_2 are also scrutinized. Firstly, we determine the most stable configuration among three possible adsorption sites, that is, one Cu adatom on the top of Mo atom (site I) or on the top of S atom (site II), and above the center of the hexagonal ring of 1L-MoS_2 (site III). The site I is found to be energetically most stable, which is favored by about 521 and 142 meV/supercell with respect to the site II and site III, respectively. In addition, for the site I, we have determined the formation enthalpy ΔH using Eq.(1). It is calculated to be -0.929 eV/atom, which is lower than that of the Cu doping at Mo site by 88 meV/atom. This is also lower than the Cu doping at S site with the difference of 28 meV/atom. The spin polarization induced by the Cu adsorption is illustrated by the spin-density distribution in Fig. 7 (b)-(d). In the figures, we describe the Cu adsorption sites on the supercell and provide the induced spin-density distributions for the site I, II, and III. As shown in the figure, in all the cases, a portion of the spin-density resides around the adsorbed Cu atom and another remnant portions are centered about neighboring Mo or S atoms. It is worthy of noting that the remnant spin polarization is induced preferably in Mo atoms than S atoms. For the most stable configuration, i.e., site I, the Cu adatom is found to have magnetic moment of 0.13 μ_B/atom, while the Mo atom just below it has the induced moment of 0.20 μ_B/atom [see Fig. 7 (b)], as listed in Table II. The total magnetic moments are now estimated to be approximately 1.0 μ_B/supercell for all the three systems, which are roughly 5 times smaller than the Cu doping at Mo site but similar to at S site.

4 Summary

In summary, we investigated the magnetic properties of the 3*d* TM doped 1L-MoS_2, i.e., with the substitutional doping of the 3*d* TM atom for the Mo atom, through the systematic first-principles electronic structure calculations. Except for Sc, Ti, and Cr doped systems, those like V, Mn, Fe, Co, Ni, Cu, and Zn doped systems are found to be magnetic. In particular, the Cu doped 1L-MoS_2 is found to have the largest total magnetic moment of 5.08 μ_B/supercell and at the same time, the largest interstitial magnetic moment of 1.06 μ_B/supercell. From the strong magnetism in the interstitial area, we attribute the magnetism of the system to a strong *p-d* hybridization between *d*

bands of the 3*d* TM and *p* bands of neighboring S atoms. Furthermore, in order to estimate the induced magnetic moment by the 3*d* TM doping, the electron-counting approach would be useful. Finally, we also made an investigation of further issues of the Cu induced magnetism such as additional charge states, the Cu doping at S site instead of Mo site, and the Cu adatom on 1L-MoS_2.

Acknowledgements

This work was supported by the Leading Foreign Research Institute Recruitment Program (Grant No. 2012K1A4A3053565) and the Basic Science Research Program (Grant No. 2013R1A1A2007388) through the National Research Foundation of Korea (NRF) funded by the Ministry of Education, Science and Technology (MEST).

References

1 J. A. Wilson and A. D. Yoffe, *Adv. Phys.*, 1969, **18**, 193-335.

2 M. Xu, T. Liang, M. Shi and H. Chen, *Chem. Rev.*, 2013, **113**, 3766-3798.

3 W. O. Winer, *Wear*, 1967, **10**, 422-452.

4 H. Topsøe, B. Hinnemann, J. K. Nørskov, J. V. Lauritsen, F. Besenbacher, P. L. Hansen, G. Hytoft, R. G. Egeberg and K. G. Knudsen, *Catal. Today*, 2005, **107-108**, 12-22.

5 X. Fang, X. Guo, Y. Mao, C. Hua, L. Shen, Y. Hu, Z. Wang, F. Wu and L. Chen, *Chem. Asian J.*, 2012, **7**, 1013-1017.

6 S. W. Han, H. Kwon, S. K. Kim, S. Ryu, W. S. Yun, D. H. Kwon, J. H. Hwang, J.-S. Kang, J. Baik, H. J. Shin and S. C. Hong, *Phys. Rev. B:Condens. Matter Mater. Phys.*, 2011, **84**, 045409.

7 A. Splendiani, L. Sun, Y. Zhang, T. Li, J. Kim, C.-Y. Chim, G. Galli and F. Wang, *Nano Lett.*, 2010, **10**, 1271-1275.

8 W. S. Yun, S. W. Han, S. C. Hong, I. G. Kim and J. D. Lee, *Phys. Rev. B:Condens. Matter Mater. Phys.*, 2012, **85**, 033305.

9 C. Espejo, T. Rangel, A. H. Romero, X. Gonze and G.-M. Rignanese, *Phys. Rev. B:Condens. Matter Mater. Phys.*, 2013, **87**, 245114.

10 K. S. Novoselov, D. Jiang, F. Schedin, T. Booth, V. V. Khotkevich, S. V. Morozov and A. K. Geim, *Proc. Natl. Acad. Sci. USA*, 2005, **102**, 10451-10453.

11 K. F. Mak, C. Lee, J. Hone, J. Shan and T. F. Heinz, *Phys. Rev. Lett.*, 2010, **105**, 136805.

12 B. Radisavljevic, A. Radenovic, J. Brivio, V. Giacometti and A. Kis, *Nat. Nanotech.*, 2011, **6**, 147-150.

13 H. S. Lee, S.-W. Min, Y.-G. Chang, M. K. Park, T. Nam, H. Kim, J. H. Kim, S. Ryu and S. Im, *Nano Lett.*, 2012, **12**, 3695-3700.

14 R. S. Sundaram, M. Engel, A. Lombardo, R. Krupke, A. C. Ferrari, Ph. Avouris and M. Steiner, *Nano Lett.*, 2013, **13**, 1416-1421.

15 Y. C. Cheng, Z. Y. Zhu, M. Tahir and U. Schwingenschlögl, *Europhys. Lett.*, 2013, **102**, 57001.

16 L.-Y. Gan, Q. Zhang, Y. Cheng and U. Schwingenschlögl, *Phys. Rev. B:Condens. Matter Mater. Phys.*, 2013, **88**, 235310.

17 Y. Li, Z. Zhou, S. Zhang and Z. J. Chen, *J. Am. Chem. Soc.*, 2008, **130**, 16739-16744.

18 A. R. Botello-Méndez, F. López-Urías, M. Terrones and H. Terrones, *Nanotechnol.*, 2009, **20**, 325703.

19 A. Vojvodic, B. Hinnemann and J. K. Norskøv, *Phys. Rev. B:Condens. Matter Mater. Phys.*, 2009, **80**, 125416.

20 J. He, K. Wu, R. Sa, Q. Li and Y. Wei, *Appl. Phys. Lett.*, 2010, **96**, 082504.

21 J. D. Fuhr, A. Saúl and J. O. Sofo, *Phys. Rev. Lett.*, 2004, **92**, 026802.

22 C. Ataca and S. Ciraci, *J. Phys. Chem. C*, 2011, **115**, 13303-13311.

23 Y. Zhou, P. Yang, H. Zu, F. Gao and X. Zu, *Phys. Chem. Chem. Phys.*, 2013, **15**, 10385-10394.

24 L. F. Seivanea, H. Barron, S. Botti, M. A. L. Marques, Á. Rubio and X. López-Lozano, *J. Mater. Res.*, 2013, **28**, 240-249.

25 S. Tongay, S. S. Vamoosfaderani, B. R. Appleton, J. Wu and A. F. Hebard, *Appl. Phys. Lett.*, 2012 **101**, 123105.

26 H.-P. Komsa, J. Kotakoski, S. Kurasch, O. Lehtinen, U. Kaiser and A. V. Krasheninnikov, *Phys. Rev. Lett.*, 2012, **109**, 035503.

27 S. Mathew, K. Gopinadhan, T. K. Chan, X. J. Yu, D. Zhan, L. Cao, A. Rusydi, M. B. H. Breese, S. Dhar, Z. X. Shen, T. Venkatesan and J. T. L. Thong, *Appl. Phys. Lett.*, 2012, **101**, 102103.

28 J. Zhang, J. M. Soon, K. P. Loh, J. Yin, J. Ding, M. B. Sullivian and P. Wu, *Nano Lett.*, 2007, **7**, 2370-2376.

29 S. W. Han, Y. H. Hwang, S.-H. Kim, W. S. Yun, J. D. Lee, M. G. Park, S. Ryu, J. S. Park, D.-H. Yoo, S.-P. Yoon, S. C. Hong, K. S. Kim and Y. S. Park, *Phys. Rev. Lett.*, 2013, **110**, 247201.

30 J. A. Rodríguez-Manzo, O. Cretu and F. Banhart, *ACS Nano*, 2010, **4**, 3422-3428.

31 X. Wei, M.-S. Wang, Y. Bando and D. Golberg, *ACS Nano*, 2010, **5**, 2916-2922.

32 H. Y. Wang, Q. Wang, Y. Cheng, K. Li, Y. Yao, Q. Zhang, C. Dong, P. Wang, U. Schwingenschlögl W. Yang and X. X. Zhang, *Nano Lett.*, 2012, **12**, 141-144.

33 Q. Yue, S. Chang, S. Qin and J. Li, *Phys. Lett. A*, 2013,

377, 1362-1367.

34 Y. C. Cheng, Z. Y. Zhu, W. B. Mi, Z. B. Guo and U. Schwingenschlögl, *Phys. Rev. B:Condens. Matter Mater. Phys.*, 2013, **87**, 100401(R).

35 A. Ramasubramaniam and D. Naveh, *Phys. Rev. B:Condens. Matter Mater. Phys.*, 2013, **87**, 195201.

36 R. Mishra, W. Zhou, S. J. Pennycook, S. T. Pantelides and J.-C. Idrobo, *Phys. Rev. B:Condens. Matter Mater. Phys.*, 2013, **88**, 144409.

37 G. Kresse and J. Furthmuller, *Phys. Rev. B:Condens. Matter Mater. Phys.*, 1996, **54**, 11169.

38 P. E. Blochl, *Phys. Rev. B:Condens. Matter Mater. Phys.*, 1994, **50**, 17953; G. Kresse and D. Joubert, *Phys. Rev. B:Condens. Matter Mater. Phys.*, 1999, **59**, 1758.

39 J. P. Perdew, K. Burke and M. Ernzerhof, *Phys. Rev. Lett.*, 1996, **77**, 3865.

40 P. A. G. O'Hare, B. M. Lewis and B. A. Parkinson, *J. Chem. Thermodynamics*, 1988, **20**, 681-691.

41 F. L. Deepak, R. Esparza, B. Borges, X. Lopez-Lozano and M. Jose-Yacaman, *ACS Catal.*, 2011, **1**, 537-543.

42 D. Kim, J. Hong, Y. R. Park and K. J. Kim, *J. Phys.:Condens. Matter*, 2009, **21**, 195405.

43 D. Kim, J. Yang and J. Hong, *J. Appl. Phys.*, 2009, **106**, 013908.

44 We have performed the same calculation using another exchange-correlation potential, i.e., local spin density approximation (LSDA). The total magnetic moment was calculated to be 4.93 μ_B/supercell, being quite close to our present GGA result and also close to the FLAPW result (4.90 μ_B/supercell).

45 K. Sato, L. Berqqvist, J. Kudrnovsky, P. H. Dederichs, O. Eriksson, I. Turek, B. Sanyal, G. Bouzerar, H. Katayama-Yoshida, V. A. Dinh, T. Fukushima, H. Kizaki and R. Zeller, *Rev. Mod. Phys.*, 2010, **82**, 1633-1690.

46 J. Kanamori and K. Terakura, *J. Phys. Soc. Jpn.*, 2001, **70**, 1433-1434.

Table 1 The calculated total magnetic moment (m_{total} in μ_B/supercell) of the 3*d* TM doped 1L-MoS_2 for both the relaxation-allowing (relaxed) and relaxation-quenching (unrelaxed) cases. Bond length ($l_{\text{TM-S}}$ in Å) between TM and S atom and bond angle (θ in degree) between TM-S bond and the planar Mo-layer are also given.

dopant	$m_{\text{total}}^{\text{relaxed}}$	$m_{\text{total}}^{\text{unrelaxed}}$	$l_{\text{TM-S}}$	θ
pristine (dopant-free)	0.00	0.00	2.41	40.76
V	0.83	0.40	2.36	40.62
Mn	1.00	1.00	2.30	41.09
Fe	2.00	2.00	2.29	40.83
Co	3.03	3.00	2.29	40.44
Ni	4.00	4.00	2.40	40.18
Cu	5.08 [44]	5.05	2.41	40.09
Zn	2.11	2.12	2.51	39.53

Table 2 The calculated magnetic moment of Cu adatom (m_{Cu} in μ_B/atom), nearest neighboring Mo atom (m_{Mo}^{NN} in μ_B/atom) and nearest neighboring S atom (m_S^{NN} in μ_B/atom), and total magnetic moment (m_{total} in μ_B/supercell) for the systems of Cu adatom adsorbed at site I, II, and III. For a case of site III, in particular, m_{Mo}^{NNN} (for the next nearest neighboring Mo atom) is larger than m_{Mo}^{NN}. m_{Mo}^{NNN} is given in parentheses.

site	m_{Cu}	m_{Mo}^{NN}	m_S^{NN}	m_{total}
I	0.13	0.20	0.01	1.07
II	0.20	0.03	0.04	1.00
III	0.13	0.04 (0.12)	0.01	1.03

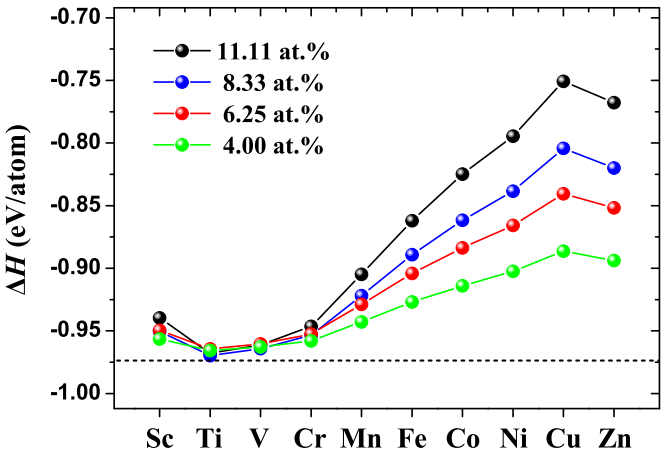

Fig. 1 ΔH of the 3*d* TM doped 1L-MoS_2 for 11.11 at.%, 8.33 at.%, 6.25 at.%, and 4 at.% concentration of TM atoms. The dotted horizontal line indicates ΔH of the pristine 1L-MoS_2.

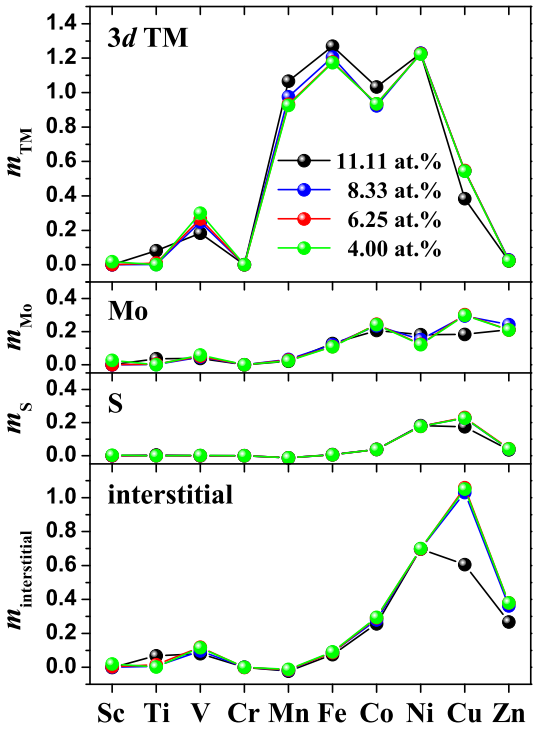

Fig. 2 Local magnetic moments (in unit of μ_B/atom) of 3*d* TM (top panel), Mo (upper middle panel), S (lower middle panel), and the interstitial magnetic moment (bottom panel) of the 3*d* TM doped 1L-MoS_2 for a series of 3*d* TM atoms at 11.11 at.%, 8.33 at.%, 6.25 at.%, and 4 at.% concentration of TM atoms.

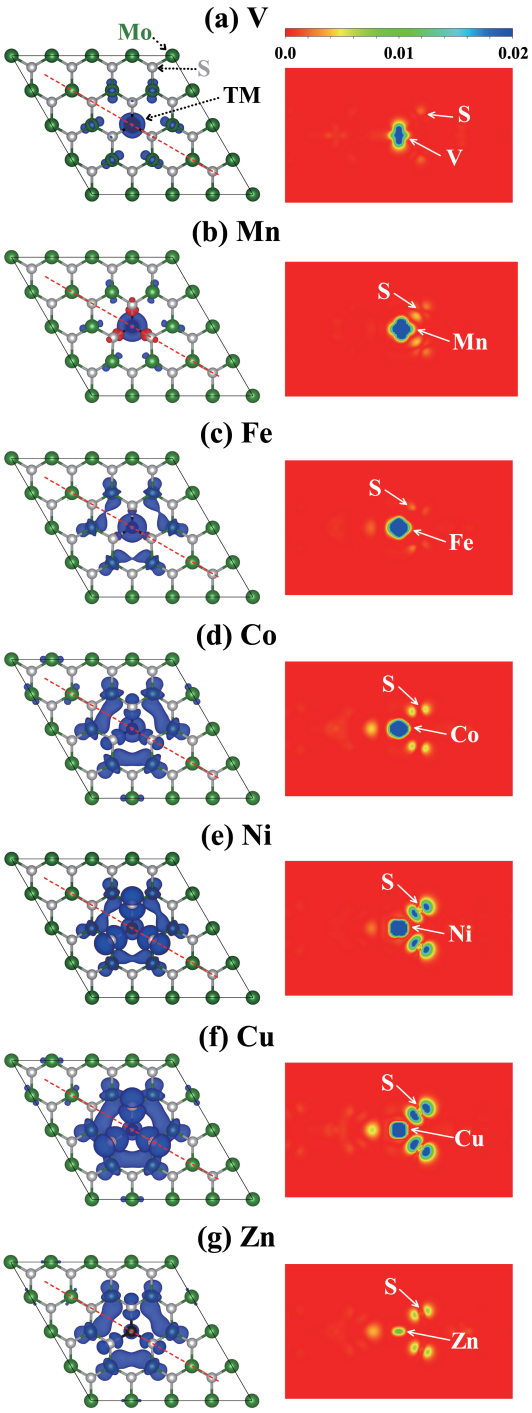

Fig. 3 Calculated spin-density isosurfaces of V, Mn, Fe, Co, Ni, Cu, and Zn doped 1L-MoS_2. The isosurface value is taken as 2×10^{-3} e/Å^3. The 4 × 4 supercell used for the calculation is represented by a black solid line. Green, gray, and black balls in left panels of (a)-(g) indicate Mo, S, and TM atoms, respectively. The blue (red) colored distribution represents the net spin-up (spin-down) electron density. Right panels of (a)-(g) describe the spin density distribution on the cross sections which are sliced along the red dashed lines of the left panels.

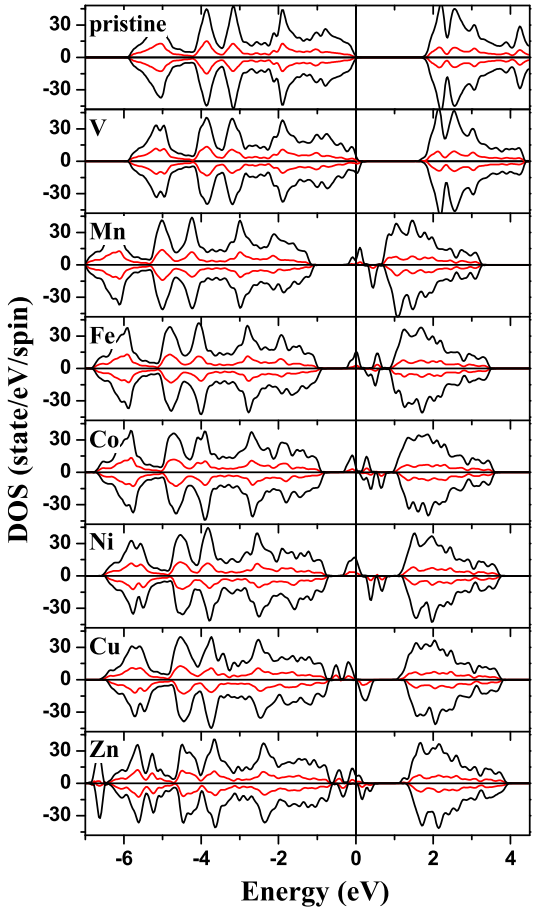

Fig. 4 Total (black solid lines) and interstitial (red solid lines) density of states (DOS) of the pristine 1L-MoS_2 and the V, Mn, Fe, Co, Ni, Cu, and Zn doped 1L-MoS_2. Positive and negative values represent the majority and minority spin bands. DOS for the pristine 1L-MoS_2 is intentionally drawn in the same fashion even if it is NM. The Fermi level is set to zero.

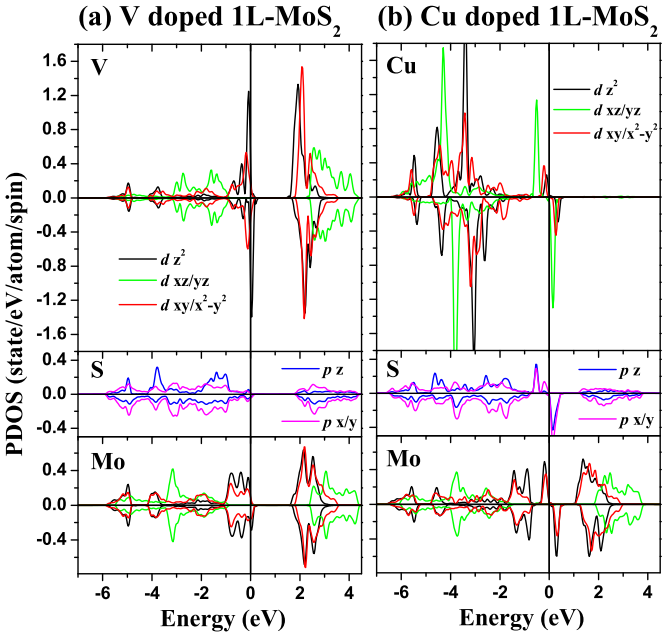

Fig. 5 Orbital-decomposed PDOS of TM (top panel) and the nearest neighbor S (middle panel) and the second-nearest neighbor Mo (bottom panel) for the (a) V and (b) Cu doped 1L-MoS_2.

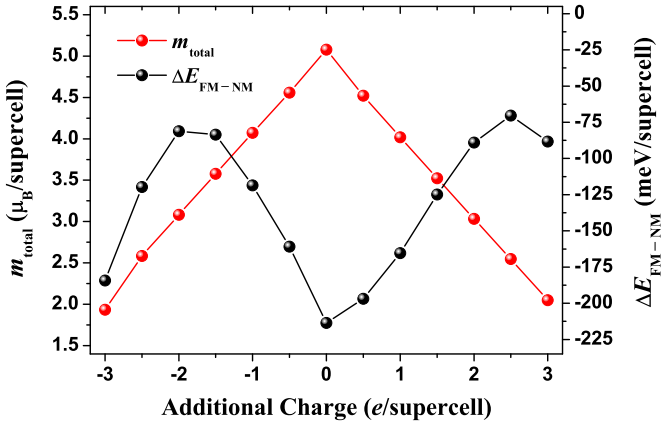

Fig. 6 Calculated total magnetic moment (left axis) and total energy difference between FM and NM states (right axis) versus the additional charge per supercell in Cu doped 1L-MoS_2. Zero electron per supercell indicates the charge-neutral state.

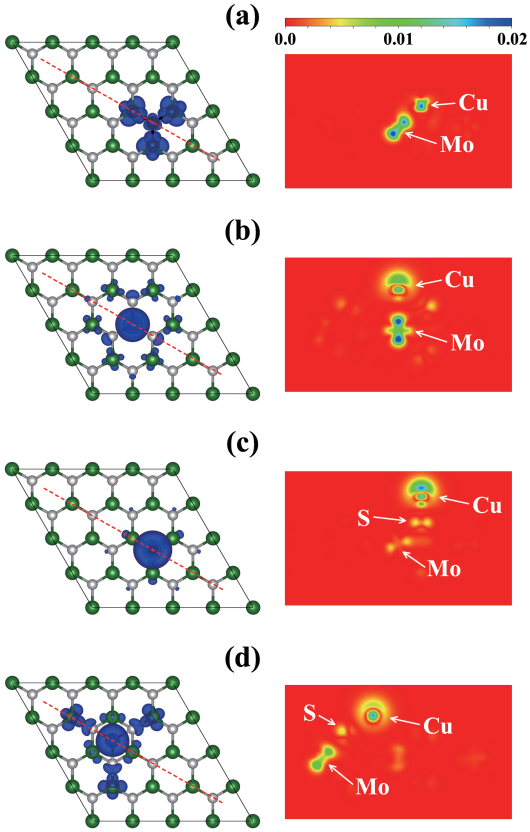

Fig. 7 Spin-density isosurfaces of 4 × 4 supercell of 1L-MoS_2 with (a) the Cu doping at S site and (b) the Cu adatom adsorbed at site I (on the top of Mo atom; the most stable configuration), (c) site II (on the top of S atom), and (d) site III (above the center of the hexagonal ring). The other notations are same as in Fig. 3.

Nonmagnetic Cu to substitute for Mo in a single-layer MoS2 induces an unexpected strong magnetism.